Planetary and Space Science 238 (2023) 105802

Contents lists available at ScienceDirect

Planetary and Space Science

journal homepage: www.elsevier.com/locate/pss

Deep machine learning for meteor monitoring: Advances with transfer learning and gradient-weighted class activation mapping

Eloy Peña-Asensio [a,b,*], Josep M. Trigo-Rodríguez [b,c], Pau Grèbol-Tomàs [b], David Regordosa-Avellana [d], Albert Rimola [a]

[a] Departament de Química, Universitat Autònoma de Barcelona, Carrer dels Til.lers, Bellaterra, 08193, Catalonia, Spain
[b] Institut de Ciències de l'Espai (ICE, CSIC), Campus UAB, C/ de Can Magrans S/N, Cerdanyola del Vallès, 08193, Catalonia, Spain
[c] Institut d'Estudis Espacials de Catalunya (IEEC), Carrer del Gran Capità, 2, Barcelona, 08034, Catalonia, Spain
[d] Spanish Meteor Network (SPMN, CSIC), Campus UAB, C/ de Can Magrans S/N, Cerdanyola del Vallès, 08193, Catalonia, Spain

ARTICLE INFO

Keywords:
Meteorites
Meteors
Meteoroids
Machine learning
Convolutional neural networks
Transfer learning

ABSTRACT

In recent decades, the use of optical detection systems for meteor studies has increased dramatically, resulting in huge amounts of data being analyzed. Automated meteor detection tools are essential for studying the continuous meteoroid incoming flux, recovering fresh meteorites, and achieving a better understanding of our Solar System. Concerning meteor detection, distinguishing false positives between meteor and non-meteor images has traditionally been performed by hand, which is significantly time-consuming. To address this issue, we developed a fully automated pipeline that uses Convolutional Neural Networks (CNNs) to classify candidate meteor detections. Our new method is able to detect meteors even in images that contain static elements such as clouds, the Moon, and buildings. To accurately locate the meteor within each frame, we employ the Gradient-weighted Class Activation Mapping (Grad-CAM) technique. This method facilitates the identification of the region of interest by multiplying the activations from the last convolutional layer with the average of the gradients across the feature map of that layer. By combining these findings with the activation map derived from the first convolutional layer, we effectively pinpoint the most probable pixel location of the meteor. We trained and evaluated our model on a large dataset collected by the Spanish Meteor Network (SPMN) and achieved a precision of 98%. Our new methodology presented here has the potential to reduce the workload of meteor scientists and station operators and improve the accuracy of meteor tracking and classification.

1. Introduction

Meteors, popularly known as shooting stars, particularly the most luminous ones called fireballs or bolides, are spectacular physical processes that have fascinated mankind for centuries (Trigo-Rodríguez, 2022). These dazzling streaks of light occur when a meteoroid enters the Earth's atmosphere at hypersonic velocity, causing intense heating through repeated collisions with air molecules (Ceplecha et al., 1998; Silber et al., 2018; Trigo-Rodríguez, 2019). Meteors are formed due to the extreme heat produced by the interaction with the gaseous environment and the rising atmospheric pressure which causes the meteoroid to undergo rapid vaporization, a process known as ablation. This ablation leads to the formation of a luminous trail composed of ionized gas and fragmented debris, which can be observed and recorded from the ground using optical devices. Current digital video imagery provides a sequential recording useful to obtain complete light curves, high temporal and spatial resolution measurements, and spectra (Hughes, 1978; Koschny et al., 2017; Subasinghe et al., 2017; Drolshagen et al., 2021).

Traditionally, two classes of meteors are considered: those that are expected to occur in a specific period of the year because they are associated with meteoroid streams, and those that are sporadic and have no discernible periodic pattern (Wiegert and Brown, 2004; Jopek and Williams, 2013; Dumitru et al., 2017; Jenniskens, 2017; Vaubaillon et al., 2019; Peña-Asensio et al., 2022, 2023). Although showers exhibit regular activity, the sporadic meteors require constant sky monitoring to quantify the meteoroid flux and properties of the different sources (Trigo-Rodríguez and Blum, 2022).

Meteors can provide valuable information about the composition, dynamics, and origin of our Solar System (Koschny et al., 2019). By analyzing the physical and chemical properties of meteorites, which are pieces of meteoroids that survive their journey through the Earth's atmosphere and land on the surface, scientists can gain insight into

* Corresponding author at: Departament de Química, Universitat Autònoma de Barcelona, Carrer dels Til.lers, Bellaterra, 08193, Catalonia, Spain.
E-mail addresses: eloy.pena@uab.cat, eloy.peas@gmail.com (E. Peña-Asensio).

https://doi.org/10.1016/j.pss.2023.105802
Received 24 May 2023; Received in revised form 4 October 2023; Accepted 25 October 2023
Available online 1 November 2023

the formation and evolution of comets and asteroids, as they provide information about the age of the Solar System, the composition of the early solar nebula, and the processes that led to the formation of the planets (Bottke et al., 2002; Lauretta and McSween, 2006).

The growing interest in meteoritics has driven an increase in the number of video meteor detection networks around the world (Ceplecha, 1987; Ceplecha et al., 1998; Koten et al., 2019; Colas et al., 2020). Comprised of strategically placed stations equipped with cameras and other sensors, these networks are designed to monitor atmospheric volumes with clear views of the sky, aiming to maximize the number of recorded meteors within common observing fields. A noteworthy trend in recent years has been the rise of pro-am collaborations in this field, involving professional scientists, amateur astronomers, and citizen scientists working together to collect valuable data. These collaborations have significantly expanded the reach of meteor networks, enabling the recording of events from diverse locations and perspectives.

However, with the increasing number of detection stations, the accumulation of video and image data has also surged. Consequently, this data influx has created a bottleneck in processing and analysis, as traditional manual methods prove to be excessively time-consuming and resource-intensive. To deal with these issues, many networks are embracing automation as a means to efficiently handle the significant volumes of generated data (Molau, 2001; Spurný et al., 2007; Gural and Šegon, 2009; Brown et al., 2010; Gural, 2011; Weryk et al., 2013; Howie et al., 2017; Suk and Šimberová, 2017; Nikolic, 2019; Peña-Asensio et al., 2021a,b; Vida et al., 2021). These automated approaches allow meteor scientists to analyze and interpret meteor data faster and more efficiently than ever before, helping to uncover new insights into meteor behavior and properties.

The detection of luminous sources moving in the sky is relatively easy to solve as the camera control software only needs to store and overwrite the last few minutes of recording, and in the event of a sudden increase in illumination, permanently save this data. However, the trigger threshold must be carefully calibrated to avoid missing any meteors while minimizing the number of false positives. Defining this cut-off is complex as it can vary depending on a number of factors, including general lighting conditions, which need to be updated periodically to consider specific dusk and dawn illumination conditions or the presence of the Moon.

The pipelines that attempt to automate the detection and tracking of meteors face a difficult task because meteors are virtually random phenomena and can occur in a variety of ways due to impact geometry, variable velocity, size, shape, composition, viewing angle, sky conditions (clouds or illumination), etc. In addition, meteors must be distinguished from false positives caused by satellites, airplanes, helicopters, drones, birds, lightning, or artificial light sources. The combination of possible characteristics that meteors can exhibit makes it difficult to define fixed parameters that work in all cases. As a result, many networks still rely on human experts to manually review the footage and identify/classify meteors. However, human operators can occasionally make errors, particularly when artificial events cause confusion or ambiguity. However, there are also networks that use fully automated approaches based on traditional computer vision techniques, such as image processing algorithms with fixed instructions, e.g. CAMS (Jenniskens et al., 2011), SonotaCo (SonotaCo, 2016), or EDMOND (Kornoš et al., 2014). Some of the detection pipelines currently in use are *MetRec*, *MeteorScan*, and *UFOCapture*; an overview of their capabilities is given in Molau and Gural (2005). These automated approaches show a high percentage of events with suspicious calculated results due to their reliance on fixed parameters that may not be appropriate for all scenarios (Hajdukova et al., 2020).

Consequently, addressing the challenges of meteor monitoring requires the adoption of artificial intelligence techniques. In this paper, we delve into the utilization of new methodologies for meteor classification and processing tasks. Specifically, we investigate how Machine Learning (ML) approaches can effectively enhance the accuracy and efficiency of automated pipelines, given the massive volume of data generated by meteor networks. We present a fully automated pipeline leveraging Convolutional Neural Networks (CNNs) for meteor detection and tracking using transfer learning and the Gradient-weighted Class Activation Mapping (Grad-CAM) technique.

2. Artificial intelligence for meteor detection

Advances in computer technology and hardware performance have fueled the remarkable progress of ML, particularly artificial neural networks with multiple layers, which are classified as deep learning. Neural networks have become increasingly popular in various domains due to their exceptional performance in image classification and recognition. Among them, CNNs have gained popularity for their fault tolerance and self-learning capabilities through multi-layer feedforward networks with a convoluted structure (Gu et al., 2018). They can handle complex environments and unclear background problems with significantly better generalization ability compared to other methods. A typical CNN architecture includes an input layer, multiple convolutional layers, pooling layers, a fully connected layer, and an output layer. CNNs can be used for both supervised and unsupervised learning, and are applied in diverse fields such as computer vision, natural language processing, and others (Hastie et al., 2001).

In the context of meteor monitoring, current research efforts using ML focus on two main objectives. First, some studies concentrate on determining the presence of a meteor in a given event, with the goal of distinguishing meteoric events from non-meteoric phenomena. Alternatively, other works rely on ML for meteor tracking, facilitating the accurate localization and monitoring of meteoroids throughout their bright atmospheric trajectory. The primary challenge is to effectively distinguish false positives caused by non-meteor objects such as airplanes, birds, and insects, or atmospheric conditions (e.g. clouds). These innovative approaches are being increasingly employed within meteor networks worldwide, including the Global Meteor Network (GMN) (Gural, 2019), AllSky7 Fireball Network Germany (FNG[1]), Meteorite Orbits Reconstruction by Optical Imaging (MOROI) (Nedelcu et al., 2018), Canadian Automated Meteor Observatory (CAMO) (Weryk et al., 2013), Cameras for All-sky Meteor Surveillance (CAMS) (Jenniskens et al., 2011), EXOSS meteor network[2], and Meteor Automatic Imager and Analyzer (MAIA) (Vítek et al., 2011).

In image classification, it is customary to use transfer learning techniques with pre-trained models of CNNs (Sennlaub et al., 2022; Marsola and Lorena, 2019; Galindo and Lorena, 2018). These methods allow inheriting the ability to detect objects from those pre-trained models, which need to be re-trained on meteors. With this methodology, optimal results are achieved with a smaller number of training data compared to starting from an uninitialized model. As underlined in Galindo and Lorena (2018), uttermost results are achieved when the proper pre-trained dataset is selected. They compared the performance of ImageNET and Fashion-MNIST (Xiao et al., 2017) with fine-tuning, concluding that the latter is the most optimal as it is already trained to work with black and white images. They also checked whether the CNN could distinguish meteors if the image was previously tweaked (slightly zoomed, rotated, or flipped). The results showed that these transformations could produce unrealistic apparent trajectories and worsen the classification. In order to solve these types of problems, Ganju et al. (2023) use a windowing technique to create new frames from existing ones. With this, all meteor detection would have the same number of frames, easing the posterior analysis. In Cecil and Campbell-Brown (2020) is shown a comparison of different sets of combinations of

[1] https://allsky7.net/.
[2] https://exoss.org/.

Table 1
Summary of the main previous works on ML applied to meteor detection. For each contribution, we denote the meteor network source, the number of samples used to train the models, their goal, the transfer learning method used (if any), the different models compared, and the best F1 score and/or accuracy achieved (when provided). F1 score and accuracy have been normalized between 0 and 1.

Article	Meteor network	# samples	Goal	Transfer learning	Model	F1 score	Accuracy
Ganju et al. (2023)	CAMS	19,152	Detection	BiLSTM	–	0.91	0.89
Anghel et al. (2023)	MOROI	9,858	Detection	–	CNN, GB and RF	0.989	0.998
Sennlaub et al. (2022)	AllSky7 FNG	20,000	Detection	ImageNET	CNN: GRU and SVM	–	0.991
Cecil and Campbell-Brown (2020)	CAMO	50,745	Tracking	No	CNN: multi-layer and max pool	0.997	0.998
Gural (2019)	CAMS	200,361	Tracking	MeteorNet	RNN and LSTM	0.974	0.981
Marsola and Lorena (2019)	EXOSS	400	Detection	ImageNET	VGG16	–	0.8435
Vítek and Nasyrova (2019)	MAIA	–	Tracking	No	DPT	–	–
Galindo and Lorena (2018)	EXOSS	1,660	Detection	Fashion-MNIST	–	0.94	0.960

different techniques used in image processing, such as convolutions and max-pools.

Even though most CNN meteor detection algorithms have been trained to reach a satisfying prediction percentage (> 99%), particularly when considering large sample sizes of more than ~10,000 events, some anomalies are still misclassified as meteors for small datasets. The next step in meteor detection algorithms is to consider the intrinsic properties of meteors on camera images to discard these misleading anomalies. Additionally, the main drawback of the current meteor tracking algorithms is the runtime required to analyze high-definition 1080p video images. However, they perform well when dealing with small, low-resolution video images.

Beyond CNNs, other ML techniques are often used. It is the case of Recurrent Neural Networks (RNN), Gradient Boost (GB), or Random Forest (RF), which can also be used as complementary analysis tools (Gural, 2019; Anghel et al., 2022). Temporal resolution can be introduced in the analysis by using other networks such as Long Short-Term Memory (LSTM), Gated Recurrent Unit (GRU), Temporal Convolutional Network (TCN), Time Delay Neural Network (TDNN), Support Vector Machine (SVM), or VGG16 (Siladi et al., 2015; Simonyan and Zisserman, 2015; Sennlaub et al., 2022), supporting 16 layers. A particular additional technique is the discrete pulse transform (DPT) (Rohwer and Laurie, 2006), in which image signals are decomposed in pulses. Vítek and Nasyrova (2019) introduced DPT to characterize the number of pulses related to the meteor compared to those of stars. Even though it is not specified if the results are better than other works, they do underline that using DPT is faster than other methods used in the MAIA data.

Sennlaub et al. (2022) also classified those false positives based on their origin. They did not achieve solid statements but pointed out similarities among false positive subgroups. As sketched in Le Lan and Dinh (2021) a future algorithm to classify the false positives would include prior knowledge of each subgroup. These could also be expanded to classify the re-entry of artificial space debris. They could also include a cross-matching identification between different stations as a method of improving the overall accuracy (Anghel et al., 2023).

Table 1 provides a comprehensive summary of the outcomes achieved in these works accompanied by the data source, the number of samples, the technique used, and the results such as F1 score and accuracy. The F1 score is a performance metric that combines precision and recall to measure the accuracy of a classification model. Precision represents the proportion of true positive predictions out of all positive predictions, while recall represents the proportion of true positive predictions out of all actual positive instances. The F1 score considers both precision and recall, making it useful when the dataset is imbalanced or when false positives and false negatives have different consequences. Accuracy is a common evaluation metric used to measure the overall correctness of a classification model. It calculates the proportion of correctly predicted instances (both true positives and true negatives) out of the total number of instances in the dataset.

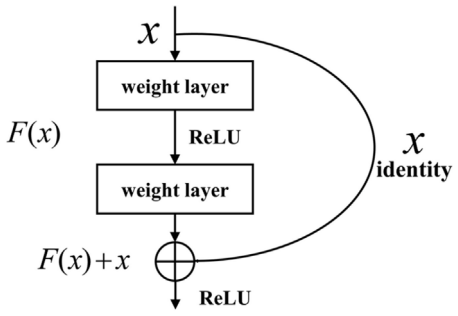

Fig. 1. A basic-block building block of ResNet-34.

3. CNN, transfer learning, and Grad-CAM

Our work aims to use ML techniques to achieve two main goals: detecting the presence of meteors in images and tracking the motion of meteors in the field of view. To achieve this, and based on the review of the scientific literature, we have decided to develop a CNN model that classifies images into two groups, "Meteors" and "No-meteors", using transfer learning. In addition, we implemented a novel application of Grad-CAM to track the coordinates of the meteor's motion.

3.1. Detection

To build our model, we chose to use ResNet-34, which is a 34-layer pre-trained CNN from the Residual Network family (He et al., 2015). This allowed us to quickly specialize the model for our specific use case using transfer learning techniques with a small dataset and rapidly inheriting all detection skills already learned by the network. ResNet-34 mainly consists of an input layer, convolutional layers, residual blocks, shortcut connections, downsampling, global average pooling, and fully connected layers. One of the key elements of this network is the residual building block, which is its infrastructure. As shown in Fig. 1, the residual building block consists of several convolutional layers (Conv), batch normalizations (BN), a rectified linear unit (ReLU) activation function, and a link. This block is used for all 34 layers of ResNet-34, as depicted in Table 2. The output of the residual block is given by the formula $y = F(x)+x$, where F is the residual function and x and y are the input and output of the residual function, respectively. The entire residual network is composed of the first convolutional layer and multiple basic blocks, making it a highly effective and efficient deep learning architecture for image recognition tasks.

For training and testing the model, we used a dataset of 982 images of meteors detected by optical devices of the Spanish Meteor Network (SPMN) network stations (Trigo-Rodríguez et al., 2006), along with 56,285 images without meteor detection collected over the year 2021, particularly from the Pujalt observatory. To balance the two groups, we generated a dataset of 982 images with meteors and 1050 without detections for training. To ensure reliable model performance, a portion of these images, specifically 20%, is allocated for validation, which is

Table 2
The structure of ResNet-34.

Layer name	Output size	34-layer
Conv1	112 × 112	$7 \times 7, 64, stride 2$ 3×3 *max pool*, $stride 2$
Conv2_x	56 × 56	$\begin{bmatrix} 3 \times 3, 64 \\ 3 \times 3, 64 \end{bmatrix} \times 3$
Conv3_x	28 × 28	$\begin{bmatrix} 3 \times 3, 128 \\ 3 \times 3, 128 \end{bmatrix} \times 4$
Conv4_x	14 × 14	$\begin{bmatrix} 3 \times 3, 256 \\ 3 \times 3, 256 \end{bmatrix} \times 6$
Conv5_x	7 × 7	$\begin{bmatrix} 3 \times 3, 512 \\ 3 \times 3, 512 \end{bmatrix} \times 3$
	1 × 1	average pool, 1000-d fc, softmax

utilized to evaluate the training progress. From this dataset, 300 images were specifically set aside for testing purposes, 150 from the meteor class and 150 from the no-meteor. The test set serves as an independent dataset to evaluate the final performance of the trained model after the completion of the training process.

The dataset consisted of grayscale long exposure (30 s) images that were pre-processed to enhance the meteor trail and remove static visual elements from the background by subtracting consecutive images. This included converting the images to black and white, resizing them to 400 × 400, and subtracting successive images to remove the background. To facilitate the generalization of the model and reduce overfitting, data augmentation techniques were used during the transfer learning process. Specifically, each batch of images received by the CNN during the 35 epochs of training was modified with geometric transformations such as randomly flipping, cropping, rotating, and translating the images, or applying lighting modifications.

3.2. Tracking

The final layer of our CNN exhibits activations corresponding to neurons that are specifically triggered when a meteor is detected in an image. While such activations provide initial utility, leveraging the subsequent classification layer's weights in conjunction with these activations further enhances their significance. It is important to note that the classification layer possesses a comprehensive understanding of the meteor classification task, enabling it to assign appropriate weights to the activated neurons. Hence, certain previously activated neurons may be deemed less influential in the final classification decision. This is the foundation of the so-called Class Activation Mapping (CAM) technique (Zhou et al., 2015).

The CAM technique is usually employed to generate a heatmap for a given class (class "meteor" in our case). This technique involves capturing the activations from the last convolutional layer of the CNN and multiplying them by the corresponding weights from the last fully connected layer responsible for the classification task. By performing this operation, the CAM technique effectively highlights the areas within the image that contribute the most to the meteor classification, that is, the Region of Interest (ROI). Fig. 2 illustrates the overall procedures of this method.

However, in order to further enhance the performance of our model, we opted to incorporate an advanced variant of CAM known as Grad-CAM (Selvaraju et al., 2016). Grad-CAM builds upon the CAM methodology by integrating gradient information instead of the weights of the classification layer. This provides a more fine-grained localization of important regions within an image. Grad-CAM computes the gradients of the target class of a specific layer with respect to the activations of the same layer. By multiplying the activations from the last convolutional layer with the average of the gradients across the feature map of that layer, Grad-CAM obtains the importance weights for the activation maps. The weighted combination of the activation maps produces the final heatmap, which visually highlights the critical regions within the input image for the classification of the target class.

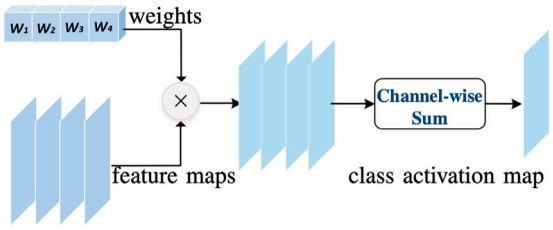

Fig. 2. The general process of class activation mapping method.
Source: Adapted from Jiang et al. (2021).

To capture finer details for properly tracking the meteor motion, we focus on the activations of the initial convolutional layer, restricting our attention to activations falling within the defined ROI delineated by the Grad-CAM. Within the CNN, the activation of the deepest layers offers a more detailed resolution map (56 × 56). However, these layers are more prone to noise and less reliable in accurately identifying the ROI related to meteor detection. To tackle these difficulties, we apply a noise reduction strategy by selectively retaining only the cells that align with the cells from the higher precision but lower resolution Grad-CAM (7 × 7) with a non-zero value. By doing so, we filter out noisy activations and focus on the cells that have a meaningful impact on the meteor classification. Subsequently, we extract the cells with the maximum activation values from the refined high-resolution activation map. By calculating the average position among these selected cells, we are able to project a single point onto the original image. This refinement process significantly enhances the accuracy of meteor detection by precisely pinpointing the location of meteors within the frames generated by our model. Fig. 3 illustrates the described meteor detection and tracking process.

Note that we do not multiply the activations of the initial layer with the weights of the classification layer because the spatial and semantic gap between the initial convolutional layer and the classification layer limits the effectiveness of such an approach. Although Grad-CAM allows the analysis of any layer in the network, we observed that focusing just on the activations from the initial convolutional layer within the ROI calculated using Grad-CAM on the last layer yields good results.

4. Training and results

Fig. 4 shows the evolution during the training process of the loss function as a function of the batches processed, which is a metric that measures the deviation between predicted and actual values. The primary goal during training is to minimize this function. The training set consists of the images used to train the CNN model, while the validation set consists of a subset of 150 images randomly selected and reserved for evaluating the model's performance and generalization ability. By evaluating the loss function on both sets, we monitor the progress of the model and detect any signs of overfitting or underfitting.

A batch refers to a group of images that are processed together during each iteration of the training algorithm. The total number of batches processed can be calculated using the formula $Batches = N * (I/BS)$, where N is the number of epochs, which is the number of times the entire training data set is passed through the network during training. I denotes the total number of images in the training dataset, including both meteor and non-meteor images. Finally, BS refers to the batch size, which represents the number of images fed to the network in each training iteration. For this study, we used a batch size of 32.

By substituting these values, we determined that a total of 1,515 batches were processed during the training process. This corresponds to the maximum value observed in Fig. 4, indicating the completion of all batches. Understanding the relationship between the loss function, the batches processed, and the progress of the training and validation sets provides valuable insight into the training dynamics and performance

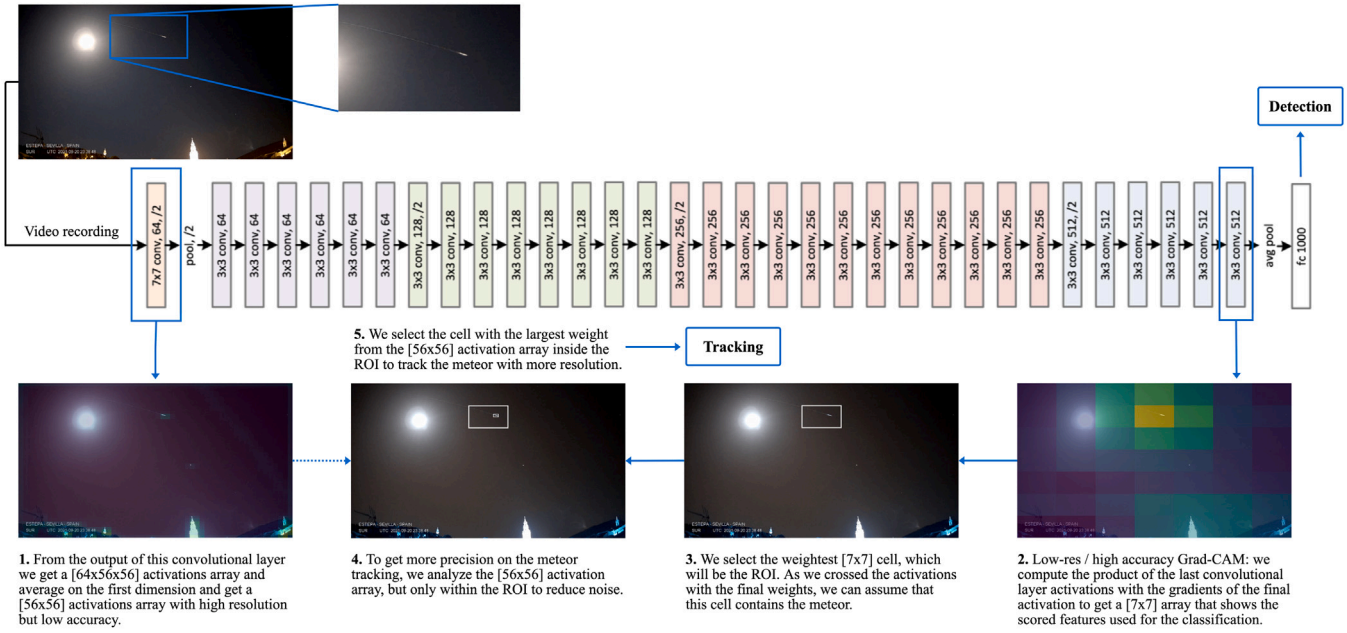

Fig. 3. Illustrative diagram of the proposed process of meteor detection and tracking using CNN and Grad-CAM. The image exemplifies a video detection made by the SPMN station in Estepa, Seville operated by Antonio J. Robles.

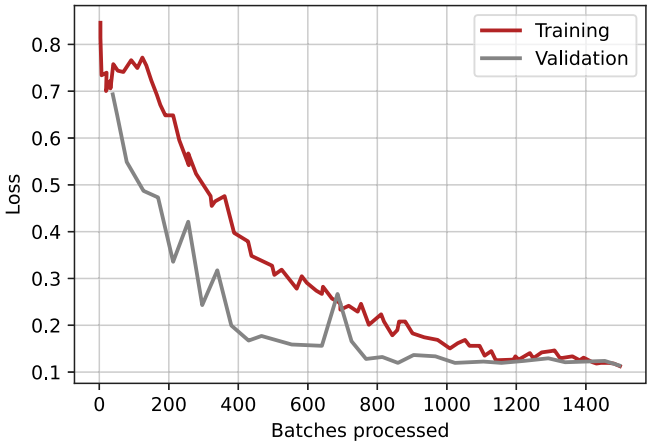

Fig. 4. Training and validation loss during model training.

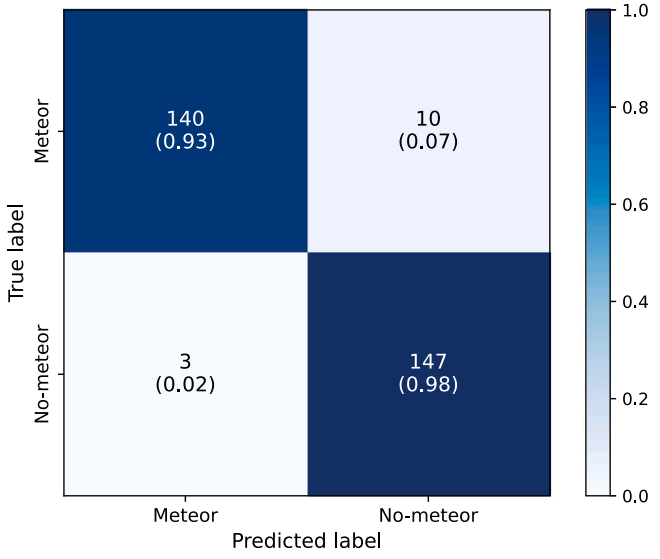

Fig. 5. Confusion matrix of the trained model with normalized values in parentheses.

evaluation of the neural network model. As every batch comprises 32 images and is subjected to various random transformations, the overall training process, including data augmentation, incorporates a varied array of 48,480 distinct images. Table 3 compiles the evolution of different metrics during the training process.

The next step involves defining the crucial hyperparameter for the training process: the learning rate. By evaluating the loss function values across various learning rates, we can identify the region of sustained and substantial loss reduction, disregarding transient peaks and irregular drops as they do not represent reliable trends. Once this region is identified, we pinpoint the midpoint of the steepest descent line, which corresponds to the most significant loss reduction. This specific learning rate is then selected for the subsequent training procedure. For our specific study, we determined a learning rate of 0.003 to be the optimal choice.

The training phase of our pipeline ends with an F1 score of 0.94, indicating the high precision and recall achieved during the training process. We then evaluated the performance of the trained model on the test dataset to assess its generalization capabilities. The evaluation results show that our model achieved an accuracy of 0.96 on the test dataset. This accuracy metric indicates the model's ability to correctly classify meteor and non-meteor images with a high degree of accuracy. Furthermore, when specifically considering the meteor class, our model achieved a precision of 0.98.

To further analyze the performance of the model, a confusion matrix was constructed as it provides insight into the classification performance by showing the distribution of the predicted labels against the true labels. The confusion matrix for our two labels "Meteor" and "No-Meteor" is shown in Fig. 5.

In the confusion matrix, the rows correspond to the true labels, while the columns represent the predicted labels. The matrix values indicate the proportion of images belonging to each category. The confusion matrix shows that 47% of the images were correctly classified as meteors, while 3.3% of the images were incorrectly classified as non-meteor images. Furthermore, 1% of the images were incorrectly

Table 3
Metrics evolution during the training process, including for each epoch the error rate, accuracy, precision, recall, and F1 score.

Epoch	Error	Accuracy	Precision	F1
0	0.245665	0.754335	0.763323	0.753592
1	0.210983	0.789017	0.788704	0.788804
2	0.205202	0.794798	0.798389	0.794714
3	0.187861	0.812139	0.823898	0.811444
4	0.127168	0.872832	0.872594	0.872726
5	0.161850	0.838150	0.842479	0.838064
6	0.104046	0.895954	0.895722	0.895867
7	0.138728	0.861272	0.875206	0.860709
8	0.086705	0.913295	0.913068	0.913222
9	0.072254	0.927746	0.928404	0.927527
10	0.063584	0.936416	0.936314	0.936382
11	0.049133	0.950867	0.950896	0.950775
12	0.060694	0.939306	0.939599	0.939294
13	0.063584	0.936416	0.936896	0.936244
14	0.049133	0.950867	0.950896	0.950775
15	0.095376	0.904624	0.912476	0.904489
16	0.066474	0.933526	0.936153	0.933521
17	0.049133	0.950867	0.950693	0.950834
18	0.052023	0.947977	0.948137	0.947865
19	0.037572	0.962428	0.962805	0.962337
20	0.052023	0.947977	0.948137	0.947865
21	0.043353	0.956647	0.956495	0.956586
22	0.052023	0.947977	0.948109	0.947961
23	0.046243	0.953757	0.953543	0.953719
24	0.037572	0.962428	0.962282	0.962375
25	0.037572	0.962428	0.962805	0.962337
26	0.049133	0.950867	0.950896	0.950775
27	0.034682	0.965318	0.965915	0.965224
28	0.043353	0.956647	0.956688	0.956566
29	0.049133	0.950867	0.950693	0.950834
30	0.049133	0.950867	0.950693	0.950834
31	0.052023	0.947977	0.947761	0.947933
32	0.046243	0.953757	0.953551	0.953702
33	0.046243	0.953757	0.953551	0.953702
34	0.034682	0.965318	0.965525	0.965244

classified as meteor images, while 49% were correctly identified as non-meteor images. The high accuracy achieved by the pipeline demonstrates its robustness in accurately detecting and classifying meteor images. The low misclassification rates for both meteor and non-meteor classes indicate the effectiveness of the trained CNNs in distinguishing between these classes, then minimizing the required human time for these time-consuming tasks.

It is worth noting that the proposed model shows the ability to generalize and accurately detect meteor trails even in color frames that have not undergone the previous frame subtraction process. This is particularly noteworthy because these frames may contain stationary elements such as clouds, the Moon, buildings, or other obstructions that can cause interference and affect the accuracy of meteor detection. Despite these challenges, the model can effectively distinguish and identify meteor trails, providing robust and reliable results. This further validates the model's ability to operate under real-world conditions, making it a valuable tool for meteor scientists and enthusiasts alike.

However, this very capability in detecting meteor trails renders it susceptible to satellite misidentifications, as they often exhibit a similar trace when reflecting the sunlight. An instance of such incorrect classification is illustrated in the top panel of Fig. 6 with a transit of a *SpaceX Starlink* satellite train, necessitating retraining the network to encompass this new class. Conversely, the bottom panel shows an undetected meteor, possibly due to its proximity to the full moon and dimming by a cloud-covered field of view.

We used data augmentation techniques during the training process, which is a common strategy that helps prevent overfitting and improves the model's ability to generalize well to unseen data. However, it is worth noting that Xiao et al. (2017) suggested data augmentation could potentially degrade model performance in certain cases. Therefore, it is possible that our use of data augmentation in the training process may have resulted in slightly lower performance compared to some of the models reported in Table 1. Despite this slight performance difference, our pipeline still demonstrates a high level of accuracy and efficiency in meteor detection and classification. The inclusion of data augmentation techniques is crucial to promote better generalization and robustness in the model, even though it may have had a slight impact on the overall results compared to other models in the comparison.

We compared our results with those obtained by Galindo and Lorena (2018) and Marsola and Lorena (2019), who used datasets of similar size to ours. In this comparison, our methodology equals or outperforms existing approaches, demonstrating superior performance. Furthermore, our pipeline incorporates the added complexity of meteor tracking, which presents a significant challenge due to the smaller luminous trace in each frame. Meteor tracking enables the computation of the velocity curve, a key factor in both discriminating between artificial and natural objects and in determining the heliocentric orbit and the potential meteorite strewn field. Automating this process facilitates the extraction of orbital elements for hundreds or thousands of meteors detected nightly, providing valuable insights into both the sporadic meteoroid background flux and the characteristics of meteoroid streams.

In subsequent phases, we intend to enhance the pipeline by refining the balance of false positives, encompassing a diverse spectrum of potential false positive sources including satellites, planes, birds, bugs, and other light sources in the training process.

5. Conclusions

The implementation of automated detection software has led to a massive increase in the amount of data collected and reduced every year by meteor networks. However, the need for human oversight to filter out false positives and organize the records has created a bottleneck, and the traditional computer vision techniques implemented have limited performance due to the random and specific characteristics of each meteor event. We employed CNNs to address these challenges.

In our study, we used a dataset of 982 meteor images along with 1,050 images without meteors detected by SPMN stations in 2021 to train a CNN model. A transfer learning technique was applied, and Grad-CAM was used for accurate tracking. Our main results are as follows:

(1) Our approach utilized ResNet-34, a deep learning architecture consisting of 34 pre-trained layers. By using pre-trained layers, we capitalized on the knowledge and representations gained from a large dataset during the initial training phase, resulting in improved model performance. In addition, data augmentation techniques were employed to facilitate the model's ability to accurately generalize and mitigate overfitting. The results achieved demonstrate a precision of 98% for meteor classification.

(2) Grad-CAM was used to track the coordinates of the meteor within each image. This technique involved analyzing deeper layers of the neural network, which have higher accuracy but lower resolution. ROI information was extracted using the gradients of the last convolutional layer and then combined with activation information from the initial layer, which is characterized by higher resolution but lower accuracy. This fusion of information allowed the identification of the most critical pixel corresponding to the position of the meteoroid. This technique allows for the precise localization of meteor positions within frames.

(3) The high performance achieved by our pipeline underscores its robustness in precisely detecting and classifying meteor images. The success rate, even with a relatively small dataset, highlights the potential of our method to significantly reduce the workload of meteor scientists and station operators involved in meteor data analysis. This potential is further enhanced by one of the most notable advancements in our methodology: the novel use of Grad-CAM for meteor tracking in combination with the initial activation map.

Fig. 6. Top panel: False positive of a *SpaceX Starlink* satellite track as it exhibits similar characteristics as a meteor trail. Recording obtained from the Alpicat SPMN station under the operation of Marc Corretgé-Gilart. Bottom panel: False negative of SPMN070523G superbolide recorded near the full moon with a cloudy sky. Recording obtained from Bartolo-Castelló SPMN station under the operation of Vicente Ibañez.

In summary, our study highlights the significant potential of applying ML techniques to meteor monitoring. It illustrates the effectiveness of CNNs and transfer learning in reducing false positives and correctly identifying meteors in images. By automating the meteor monitoring process, our pipeline increases the efficiency of meteor detection and tracking using the Grad-CAM technique. This, in turn, facilitates the study of meteoroid fluxes, aids in population characterization, and improves our ability to distinguish between meteorite-dropping events, thereby increasing fresh extraterrestrial material recovery rates.

CRediT authorship contribution statement

Eloy Peña-Asensio: Conceptualization, Methodology, Writing. **Josep M. Trigo-Rodríguez:** Supervision, Project administration. **Pau Grèbol-Tomàs:** Investigation, Resources. **David Regordosa-Avellana:** Conceptualization, Methodology, Software. **Albert Rimola:** Funding acquisition, Supervision.

Declaration of competing interest

The authors declare that they have no known competing financial interests or personal relationships that could have appeared to influence the work reported in this paper.

Data availability

Data will be made available on request.

Acknowledgments

This project has received funding from the European Research Council (ERC) under the European Union's Horizon 2020 research and innovation programme (grant agreement No. 865657) for the project "Quantum Chemistry on Interstellar Grains" (QUANTUMGRAIN). JMT-R, EP-A, and PG-T acknowledge financial support from the project PID2021-128062NB-I00 funded by MCIN/AEI/10.13039/5011000 11033. AR acknowledges financial support from the FEDER/Ministerio de Ciencia e Innovación – Agencia Estatal de Investigación (PID2021-126427NB-I00, PI: AR). This work was also partially supported by the program Unidad de Excelencia María de Maeztu CEX2020-001058-M. We thank all SPMN station operators and photographers whose continuous dedication has allowed to record incessantly the meteors of the Iberian Peninsula, the Balearic Islands, and the Canary Islands. We express our gratitude to David Puiggròs-Figueras for his assistance in the CAM and Grad-CAM methodology. The following *Python* packages were extensively used in the study: *Numpy*, *OpenCV*, *Matplotlib*, *PyTorch*, and *fast.ai*.

References

Anghel, S., Nedelcu, D.-A., Birlan, M., Boaca, I., 2022. Machine learning methods applied to meteor detection filtering. In: European Planetary Science Congress. http://dx.doi.org/10.5194/epsc2022-1107, EPSC2022–1107.

Anghel, S., Nedelcu, D.A., Birlan, M., Boaca, I., 2023. Single-station meteor detection filtering using machine learning on MOROI data. Mon. Not. R. Astron. Soc. 518 (2), 2810–2824. http://dx.doi.org/10.1093/mnras/stac3229.

Bottke, W.F., Cellino, A., Paolicchi, P., Binzel, R.P. (Eds.), 2002. Asteroids III. University of Arizona Press, http://dx.doi.org/10.2307/j.ctv1v7zdn4.

Brown, P., Weryk, R.J., Kohut, S., Edwards, W.N., Krzeminski, Z., 2010. Development of an all-sky video meteor network in southern ontario, Canada the ASGARD system. WGN, J. Int. Meteor Organ. 38 (1), 25–30.

Cecil, D., Campbell-Brown, M., 2020. The application of convolutional neural networks to the automation of a meteor detection pipeline. Planet. Space Sci. 186, 104920. http://dx.doi.org/10.1016/j.pss.2020.104920.

Ceplecha, Z., 1987. Geometric, dynamic, orbital and photometric data on meteoroids from photographic fireball networks. Bull. Astron. Inst. Czech. 38, 222.

Ceplecha, Z., Borovička, J., Elford, W.G., Revelle, D.O., Hawkes, R.L., Porubčan, V., Šimek, M., 1998. Meteor phenomena and bodies. Space Sci. Rev. 84, 327–471. http://dx.doi.org/10.1023/A:1005069928850.

Colas, F., Zanda, B., Bouley, S., Jeanne, S., Malgoyre, A., Birlan, M., Blanpain, C., Gattacceca, J., Jorda, L., Lecubin, R., Zollo, A., 2020. FRIPON: A worldwide network to track incoming meteoroids. Astron. Astrophys. 644, A53. http://dx.doi.org/10.1051/0004-6361/202038649, arXiv:2012.00616.

Drolshagen, E., Ott, T., Koschny, D., Drolshagen, G., Vaubaillon, J., Colas, F., Zanda, B., Bouley, S., Jeanne, S., Malgoyre, A., Birlan, M., Vernazza, P., Gardiol, D., Nedelcu, D.A., Rowe, J., Forcier, M., Trigo-Rodriguez, J.M., Peña-Asensio, E., Lamy, H., Ferrière, L., Barghini, D., Carbognani, A., Di Martino, M., Rasetti, S., Valsecchi, G.B., Volpicelli, C.A., Di Carlo, M., Knapic, C., Pratesi, G., Riva, W., Stirpe, G.M., Zorba, S., Hernandez, O., Grandchamps, A., Jehin, E., Jobin, M., King, A., Sanchez-Lavega, A., Toni, A., Rimola, A., Poppe, B., 2021. Luminous efficiency based on FRIPON meteors and limitations of ablation models. Astron. Astrophys. 650, A159. http://dx.doi.org/10.1051/0004-6361/202040204.

Dumitru, B.A., Birlan, M., Popescu, M., Nedelcu, D.A., 2017. Association between meteor showers and asteroids using multivariate criteria. Astron. Astrophys. 607, A5. http://dx.doi.org/10.1051/0004-6361/201730813.

Galindo, Y., Lorena, A.C., 2018. Deep Transfer Learning for Meteor Detection. In: Anais Do XV Encontro Nacional de InteligÊncia Artificial E Computacional (ENIAC 2018). Sociedade Brasileira de Computação - SBC, São Paulo, pp. 528–537. http://dx.doi.org/10.5753/eniac.2018.4445, URL http://portaldeconteudo.sbc.org.br/index.php/eniac/article/view/4445.

Ganju, S., Hatua, A., Jenniskens, P., Krishna, S., Ren, C., Ambardar, S., 2023. AI-enhanced data processing and discovery crowd sourcing for meteor shower mapping. http://dx.doi.org/10.48550/ARXIV.2308.02664, URL https://arxiv.org/abs/2308.02664.

Gu, J., Wang, Z., Kuen, J., Ma, L., Shahroudy, A., Shuai, B., Liu, T., Wang, X., Wang, G., Cai, J., Chen, T., 2018. Recent advances in convolutional neural networks. Pattern Recognit. 77, 354–377. http://dx.doi.org/10.1016/j.patcog.2017.10.013.

Gural, P.S., 2011. The california all-sky meteor surveillance (CAMS) system. In: Proceedings of the International Meteor Conference, 29th IMC, Armagh, Northern Ireland, 2010. pp. 28–31.

Gural, P.S., 2019. Deep learning algorithms applied to the classification of video meteor detections. Mon. Not. R. Astron. Soc. 489 (4), 5109–5118. http://dx.doi.org/10.1093/mnras/stz2456.

Gural, P., Šegon, D., 2009. A new meteor detection processing approach for observations collected by the Croatian meteor network (CMN). WGN, J. Int. Meteor Organ. 37 (1), 28–32.

Hajdukova, M., Sterken, V., Wiegert, P., Kornoš, L., 2020. The challenge of identifying interstellar meteors. Planet. Space Sci. 192, 105060. http://dx.doi.org/10.1016/j.pss.2020.105060.

Hastie, T., Friedman, J., Tibshirani, R., 2001. The Elements of Statistical Learning. Springer, New York, http://dx.doi.org/10.1007/978-0-387-21606-5.

He, K., Zhang, X., Ren, S., Sun, J., 2015. Deep residual learning for image recognition. http://dx.doi.org/10.48550/arXiv.1512.03385, arXiv e-prints, arXiv:1512.03385, arXiv:1512.03385.

Howie, R.M., Paxman, J., Bland, P.A., Towner, M.C., Cupak, M., Sansom, E.K., Devillepoix, H.A.R., 2017. How to build a continental scale fireball camera network. Exp. Astron. 43 (3), 237–266. http://dx.doi.org/10.1007/s10686-017-9532-7.

Hughes, D.W., 1978. Meteors. In: McDonnell, J.A.M. (Ed.), Cosmic Dust. pp. 123–185.

Jenniskens, P., 2017. Meteor showers in review. Planet. Space Sci. 143, 116–124. http://dx.doi.org/10.1016/j.pss.2017.01.008.

Jenniskens, P., Gural, P.S., Dynneson, L., Grigsby, B.J., Newman, K.E., Borden, M., Koop, M., Holman, D., 2011. CAMS: Cameras for allsky meteor surveillance to establish minor meteor showers. Icarus 216 (1), 40–61. http://dx.doi.org/10.1016/j.icarus.2011.08.012.

Jenniskens, P., Gural, P., Dynneson, L., Grigsby, B., Newman, K., Borden, M., Koop, M., Holman, D., 2011. CAMS: Cameras for allsky meteor surveillance to establish minor meteor showers. Icarus 216 (1), 40–61. http://dx.doi.org/10.1016/j.icarus.2011.08.012, URL https://www.sciencedirect.com/science/article/pii/S0019103511003290.

Jiang, P.-T., Zhang, C.-B., Hou, Q., Cheng, M.-M., Wei, Y., 2021. Layercam: Exploring hierarchical class activation maps for localization. IEEE Trans. Image Process. 30, 5875–5888. http://dx.doi.org/10.1109/TIP.2021.3089943.

Jopek, T.J., Williams, I.P., 2013. Stream and sporadic meteoroids associated with near-earth objects. Mon. Not. R. Astron. Soc. 430 (3), 2377–2389. http://dx.doi.org/10.1093/mnras/stt057.

Kornoš, L., Koukal, J., Piffl, R., Tóth, J., 2014. EDMOND meteor database. In: Gyssens, M., Roggemans, P., Zoladek, P. (Eds.), Proceedings of the International Meteor Conference, Poznan, Poland, 22-25 August 2013. pp. 23–25.

Koschny, D., Drolshagen, E., Drolshagen, S., Kretschmer, J., Ott, T., Drolshagen, G., Poppe, B., 2017. Flux densities of meteoroids derived from optical double-station observations. Planet. Space Sci. 143, 230–237. http://dx.doi.org/10.1016/j.pss.2016.12.007.

Koschny, D., Soja, R.H., Engrand, C., Flynn, G.J., Lasue, J., Levasseur-Regourd, A.-C., Malaspina, D., Nakamura, T., Poppe, A.R., Sterken, V.J., Trigo-Rodríguez, J.M., 2019. Interplanetary dust, meteoroids, meteors and meteorites. Space Sci. Rev. 215 (4), 34. http://dx.doi.org/10.1007/s11214-019-0597-7.

Koten, P., Rendtel, J., Shrbený, L., Gural, P., Borovička, J., Kozak, P., 2019. Meteors and meteor showers as observed by optical techniques. In: Ryabova, G.O., Asher, D.J., Campbell-Brown, M.J. (Eds.), Meteoroids: Sources of Meteors on Earth and beyond. p. 90.

Lauretta, D.S., McSween, H.Y. (Eds.), 2006. Meteorites and the Early Solar System II. University of Arizona Press, http://dx.doi.org/10.2307/j.ctv1v7zdmm.

Le Lan, C., Dinh, L., 2021. Perfect Density Models Cannot Guarantee Anomaly Detection. Entropy 23 (12), 1690. http://dx.doi.org/10.3390/e23121690, URL https://www.mdpi.com/1099-4300/23/12/1690.

Marsola, T.C.L., Lorena, A.C., 2019. Meteor detection using deep convolutional neural networks. In: Anais do 14% Simpósio Brasileiro de Automação Inteligente.

Molau, S., 2001. The AKM video meteor network. In: Warmbein, B. (Ed.), Meteoroids 2001 Conference. In: ESA Special Publication, vol. 495, pp. 315–318.

Molau, S., Gural, P.S., 2005. A review of video meteor detection and analysis software. WGN, J. Int. Meteor Organ. 33 (1), 15–20.

Nedelcu, A.D., Birlan, M., Turcu, V., Badescu, O., Boaca, I., Gornea, A., Blagoi, O., Danescu, C., Paraschiv, P., 2018. The MOROI network. Meteorites orbits reconstruction by optical imaging. In: ZAC 2018 - International Conference Outlook in Astronomy. p. 21.

Nikolic, V., 2019. Automation of a video meteor network. In: Rudawska, R., Rendtel, J., Powell, C., Lunsford, R., Verbeeck, C., Knofel, A. (Eds.), International Meteor Conference, Pezinok-Modra, Slovakia. pp. 139–140.

Peña-Asensio, E., Trigo-Rodríguez, J.M., Gritsevich, M., Rimola, A., 2021a. Accurate 3D fireball trajectory and orbit calculation using the 3D-FIRETOC automatic python code. Mon. Not. R. Astron. Soc. 504 (4), 4829–4840. http://dx.doi.org/10.1093/mnras/stab999, arXiv:2103.13758.

Peña-Asensio, E., Trigo-Rodríguez, J.M., Langbroek, M., Rimola, A., Robles, A.J., 2021b. Using fireball networks to track more frequent reentries: Falcon 9 upper-stage orbit determination from video recordings. Astrodynamics 5 (4), 347–358. http://dx.doi.org/10.1007/s42064-021-0112-2, arXiv:2109.01004.

Peña-Asensio, E., Trigo-Rodríguez, J.M., Rimola, A., 2022. Orbital characterization of superbolides observed from space: Dynamical association with near-earth objects, meteoroid streams, and identification of hyperbolic meteoroids. Astron. J. 164 (3), 76. http://dx.doi.org/10.3847/1538-3881/ac75d2, arXiv:2206.03115.

Peña-Asensio, E., Trigo-Rodríguez, J.M., Rimola, A., Corretgé-Gilart, M., Koschny, D., 2023. Identifying meteorite droppers among the population of bright 'sporadic' bolides imaged by the spanish meteor network during the spring of 2022. Mon. Not. R. Astron. Soc. 520 (4), 5173–5182. http://dx.doi.org/10.1093/mnras/stad102, arXiv:2301.03515.

Rohwer, C.H., Laurie, D.P., 2006. The discrete pulse transform. SIAM J. Math. Anal. 38, 1012–1034.

Selvaraju, R.R., Das, A., Vedantam, R., Cogswell, M., Parikh, D., Batra, D., 2016. Grad-CAM: Why did you say that?. http://dx.doi.org/10.48550/ARXIV.1611.07450, URL https://arxiv.org/abs/1611.07450.

Sennlaub, R., Hofmann, M., Hankey, M., Ennes, M., Müller, T., Kroll, P., Mäder, P., 2022. Object classification on video data of meteors and meteor-like phenomena: algorithm and data. Mon. Not. R. Astron. Soc. 516 (1), 811–823. http://dx.doi.org/10.1093/mnras/stac1948, arXiv:2208.14914.

Siladi, E., Vida, D., Nyarko, K., 2015. Video meteor detection filtering using soft computing methods. In: International Meteor Conference Mistelbach, Austria. p. 24.

Silber, E.A., Boslough, M., Hocking, W.K., Gritsevich, M., Whitaker, R.W., 2018. Physics of meteor generated shock waves in the earth's atmosphere - A review. Adv. Space Res. 62 (3), 489–532. http://dx.doi.org/10.1016/j.asr.2018.05.010, arXiv:1805.07842.

Simonyan, K., Zisserman, A., 2015. Very Deep Convolutional Networks for Large-Scale Image Recognition. URL http://arxiv.org/abs/1409.1556, cs.

SonotaCo, 2016. Observation error propagation on video meteor orbit determination. WGN, J. Int. Meteor Organ. 44 (2), 42–45.

Spurný, P., Borovička, J., Shrbený, L., 2007. Automation of the czech part of the European fireball network: equipment, methods and first results. In: Valsecchi, G.B., Vokrouhlický, D., Milani, A. (Eds.), Near Earth Objects, Our Celestial Neighbors: Opportunity and Risk, Vol. 236. pp. 121–130. http://dx.doi.org/10.1017/S1743921307003146.

Subasinghe, D., Campbell-Brown, M., Stokan, E., 2017. Luminous efficiency estimates of meteors -I. Uncertainty analysis. Planet. Space Sci. 143, 71–77. http://dx.doi.org/10.1016/j.pss.2016.12.009, arXiv:1704.08656.

Suk, T., Šimberová, S., 2017. Automated meteor detection by all-sky digital camera systems. Earth Moon Planets 120 (3), 189–215. http://dx.doi.org/10.1007/s11038-017-9511-z.

Trigo-Rodríguez, J.M., 2019. The flux of meteoroids over time: meteor emission spectroscopy and the delivery of volatiles and chondritic materials to earth. In: Hypersonic Meteoroid Entry Physics. IOP Publishing, p. 4. http://dx.doi.org/10.1088/2053-2563/aae894ch4.

Trigo-Rodríguez, J.M., 2022. Asteroid Impact Risk: Impact Hazard from Asteroids and Comets. Springer Nature, p. 126.

Trigo-Rodríguez, J.M., Blum, J., 2022. Learning about comets from the study of mass distributions and fluxes of meteoroid streams. Mon. Not. R. Astron. Soc. 512 (2), 2277–2289. http://dx.doi.org/10.1093/mnras/stab2827, arXiv:2109.14428.

Trigo-Rodríguez, J.M., Llorca, J., Castro-Tirado, A.J., Ortiz, J.L., Docobo, J.A., Fabregat, J., 2006. The spanish fireball network. Astron. Geophys. 47 (2), 6.26–6.28. http://dx.doi.org/10.1111/j.1468-4004.2006.47626.x.

Vaubaillon, J., Neslušan, L., Sekhar, A., Rudawska, R., Ryabova, G.O., 2019. From parent body to meteor shower: The dynamics of meteoroid streams. In: Ryabova, G.O., Asher, D.J., Campbell-Brown, M.J. (Eds.), Meteoroids: Sources of Meteors on Earth and beyond. Cambridge University Press., p. 161.

Vida, D., Šegon, D., Gural, P.S., Brown, P.G., McIntyre, M.J.M., Dijkema, T.J., Pavletić, L., Kukić, P., Mazur, M.J., Eschman, P., Roggemans, P., Merlak, A., Zubović, D., 2021. The global meteor network - methodology and first results. Mon. Not. R. Astron. Soc. 506 (4), 5046–5074. http://dx.doi.org/10.1093/mnras/stab2008, arXiv:2107.12335.

Vítek, S., Fliegel, K., Páta, P., Koten, P., 2011. MAIA: Technical development of a novel system for video observations of meteors. Acta Polytech. 51 (1), http://dx.doi.org/10.14311/1340.

Vítek, S., Nasyrova, M., 2019. Fast meteor tracking in noisy video sequences. Astron. Nachr. 340 (7), 646–651. http://dx.doi.org/10.1002/asna.201913670.

Weryk, R.J., Campbell-Brown, M.D., Wiegert, P.A., Brown, P.G., Krzeminski, Z., Musci, R., 2013. The Canadian automated meteor observatory (CAMO): System overview. Icarus 225 (1), 614–622. http://dx.doi.org/10.1016/j.icarus.2013.04.025.

Weryk, R., Campbell-Brown, M., Wiegert, P., Brown, P., Krzeminski, Z., Musci, R., 2013. The Canadian automated meteor observatory (CAMO): System overview. Icarus 225 (1), 614–622. http://dx.doi.org/10.1016/j.icarus.2013.04.025, URL https://www.sciencedirect.com/science/article/pii/S0019103513001905.

Wiegert, P., Brown, P., 2004. The problem of linking minor meteor showers to their parent bodies: initial considerations. Earth Moon Planets 95 (1–4), 19–26. http://dx.doi.org/10.1007/s11038-005-4342-8.

Xiao, H., Rasul, K., Vollgraf, R., 2017. Fashion-MNIST: A Novel Image Dataset for Benchmarking Machine Learning Algorithms. URL http://arxiv.org/abs/1708.07747, cs,stat.

Zhou, B., Khosla, A., Lapedriza, A., Oliva, A., Torralba, A., 2015. Learning deep features for discriminative localization. http://dx.doi.org/10.48550/arXiv.1512.04150, arXiv e-prints, arXiv:1512.04150, arXiv:1512.04150.